RSNA Journals > CME > Subscribe Subscribe Email Alerts
RadioGraphics
Author Instructions | Current Issue | All Issues | Collections > | Collections A-Z | Subscribe | Advertising | Contact Us | Submit a Manuscript
Home > RadioGraphics > Vol. 40, No. 2 >
< PREVIOUS NEXT >
Pediatric Imaging
Review Article
MRI of Rhabdomyosarcoma and Other Soft Tissue Sarcomas in Children
Thomas J. Vogl, Gerwin P. Dietrich, Sven Dorsch, Ralf Kaiser, Ralf Kaiser, Ralf Kaiser

Download as PowerPoint | Open in Image Viewer

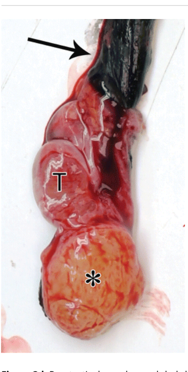

Figure 3d. Paratesticular embryonal rhabdomyosarcoma involving the left hemiscrotum in a 4-year-old boy. **(a)** Sagittal T2-weighted image shows a heterogeneously hyperintense intrascrotal round lesion (*) with no clear plane of separation (arrow) from the adjacent testicle *(T)*. *B* = bladder. **(b)** Axial T1-weighted image shows that the mass (*) is predominantly isointense to muscle, although it contains small hyperintense foci (arrow), which may represent hemorrhage. **(c)** Left: Image from volumetric determination of ADC shows a tumor volume of 6 mL with ADC of 1.5 × 10^{-3} mm^2/sec. Right: The ADC histogram is high and sharp. **(d)** Photograph of the surgical specimen shows a yellowish tumor (*) with abundant myxoid component, which correlates with high ADC. The spermatic cord is dark (arrow) owing to postsurgical hemorrhage. *T* = testis.

Download as PowerPoint | Open in Image Viewer

***Histopathologic Findings.*—**Embryonal rhabdomyosarcoma arises from undifferentiated mesenchyme, which displays features of embryonic skeletal myogenesis. It is composed of primitive poorly differentiated mesenchymal cells with different patterns (23,32). Nuclear expression of MyoD1 and myogenin is characteristic and highly specific for rhabdomyosarcoma.

***Conventional MRI Findings.*—**Embryonal rhabdomyosarcoma in the neck is typically a large and heterogeneous mass associated with regional lymphadenopathy (Fig 4). The mass is typically iso- to hyperintense to muscle on T1-weighted images and heterogeneously hyperintense to muscle on T2-weighted images owing to hemorrhage or necrosis (5) (Table 6). It shows inhomogeneous enhancement after contrast material injection (5,24).

Figure 4a. Embryonal rhabdomyosarcoma involving the parapharyngeal space in a 7-year-old boy. **(a)** Axial T2-weighted image shows a heterogeneously hyperintense lobulated mass (arrow) in the right parapharyngeal space. **(b)** Axial T2-weighted image 1 month after treatment shows decrease in size of the mass (arrow). **(c)** Images from volumetric determination of ADC show initial tumor volume of 33 mL (left) and volume after 1 month of treatment of 18 mL (right). **(d)** Graphs from volumetric determination of ADC before treatment show ADC of 0.77 × 10^{-3} mm^2/sec with a high and sharp ADC histogram (large arrow). The ADC after one cycle of chemotherapy was 1.09 × 10^{-3} mm^2/sec with a corresponding short and wide ADC histogram with rightward shift (small arrow).

Download as PowerPoint | Open in Image Viewer

Figure 4b. Embryonal rhabdomyosarcoma involving the parapharyngeal space in a 7-year-old boy. **(a)** Axial T2-weighted image shows a heterogeneously hyperintense lobulated mass (arrow) in the right parapharyngeal space. **(b)** Axial T2-weighted image 1 month after treatment shows decrease in size of the mass (arrow). **(c)** Images from volumetric determination of ADC show initial tumor volume of 33 mL (left) and volume after 1 month of treatment of 18 mL (right). **(d)** Graphs from volumetric determination of ADC before treatment show ADC of 0.77 × 10^{-3} mm^2/sec with a high and sharp ADC histogram (large arrow). The ADC after one cycle of chemotherapy was 1.09 × 10^{-3} mm^2/sec with a corresponding short and wide ADC histogram with rightward shift (small arrow).

Download as PowerPoint | Open in Image Viewer

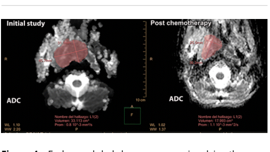

Figure 4c. Embryonal rhabdomyosarcoma involving the parapharyngeal space in a 7-year-old boy. **(a)** Axial T2-weighted image shows a heterogeneously hyperintense lobulated mass (arrow) in the right parapharyngeal space. **(b)** Axial T2-weighted image 1 month after treatment shows decrease in size of the mass (arrow). **(c)** Images from volumetric determination of ADC show initial tumor volume of 33 mL (left) and volume after 1 month of treatment of 18 mL (right). **(d)** Graphs from volumetric determination of ADC before treatment show ADC of 0.77 × 10^{-3} mm^2/sec with a high and sharp ADC histogram (large arrow). The ADC after one cycle of chemotherapy was 1.09 × 10^{-3} mm^2/sec with a corresponding short and wide ADC histogram with rightward shift (small arrow).

Download as PowerPoint | Open in Image Viewer

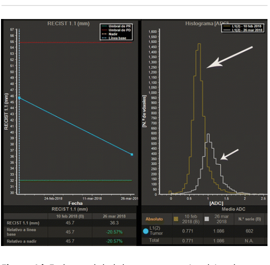

Figure 4d. Embryonal rhabdomyosarcoma involving the parapharyngeal space in a 7-year-old boy. **(a)** Axial T2-weighted image shows a heterogeneously hyperintense lobulated mass (arrow) in the right parapharyngeal space. **(b)** Axial T2-weighted image 1 month after treatment shows decrease in size of the mass (arrow). **(c)** Images from volumetric determination of ADC show initial tumor volume of 33 mL (left) and volume after 1 month of treatment of 18 mL (right). **(d)** Graphs from volumetric determination of ADC before treatment show ADC of 0.77 × 10^{-3} mm^2/sec with a high and sharp ADC histogram (large arrow). The ADC after one cycle of chemotherapy was 1.09 × 10^{-3} mm^2/sec with a corresponding short and wide ADC histogram with rightward shift (small arrow).

Download as PowerPoint | Open in Image Viewer

Table 6: MRI Features of Soft-Tissue Sarcomas in Children

Table 6: MRI Features of Soft-Tissue Sarcomas in Children

Sarcoma Type and Subtype	Location	MRI Appearance: T1W	T2W	T1W FS + CE	DWI Diffusion	DCE Curve Profiles
Embryonal rhabdomyosarcoma						
Spindle cell	Head and neck	Iso- to hyperintense to muscle	Heterogeneously hyperintense to muscle owing to necrosis or hemorrhage	Heterogeneous enhancement due to necrosis	Restricted in solid areas; no restriction in areas of necrosis or hemorrhage	Type III or IV in solid areas; type I in necrotic areas
	Retroperitoneum	Predominantly hypointense to muscle owing to necrosis	Heterogeneously hyperintense to muscle owing to necrosis or hemorrhage	Heterogeneous enhancement due to necrosis	Restricted in solid areas; no restriction in areas of necrosis or hemorrhage	Type III or IV in solid areas; type I in necrotic areas
	Paratesticular	Isointense to testicle	Heterogeneously hyperintense to testicle	Heterogeneous enhancement	No restriction owing to necrosis or myxoid component	Type III or IV
Botryoid	Bladder, prostate, vagina, biliary tree	Iso- to hyperintense to muscle	Heterogeneously hyperintense to muscle owing to necrosis or hemorrhage	Internal vascularization decreases with tumor growth owing to internal necrosis	Restricted in solid areas; no restriction in areas of necrosis or hemorrhage	Type III or IV in solid areas; type I in necrotic areas
Alveolar rhabdomyosarcoma	Extremities, trunk	Iso- to hyperintense to muscle Erosions	Heterogeneously hyperintense to muscle Fascial involvement	Heterogeneous enhancement	Restricted	Type III or IV
MPNST	Extremities	Isointense to muscle	Perilesion edema-like zone and intratumor necrosis	Peripheral enhancement pattern	Restricted in solid areas; no restriction in areas of necrosis or hemorrhage	Type III or IV in solid areas; type I in necrotic areas
Synovial sarcoma	Lower extremity around knee	Heterogeneous internal signal intensity	Heterogeneous internal signal intensity "Triple signal intensity" sign	Heterogeneous enhancement due to internal necrosis, hemorrhage, calcification, and cystic areas	Restricted in solid areas; no restriction in areas of necrosis or hemorrhage	Type III or IV in solid areas; type I in necrotic areas
Extraosseous Ewing sarcoma	Lower extremity	Hypo- to isointense	High signal intensity Microcystic appearance	Heterogeneous enhancement with internal foci of necrosis	Restricted	Type III or IV
Infantile fibrosarcoma	Extremities	Hypo- to isointense Cortical thickening, bending deformities, and erosions	Hyperintense	Heterogeneous enhancement	Restricted owing to high cellularity	Type III or IV
Epithelioid sarcoma	Hand, wrist	Homogeneously isointense	Homogeneously hyperintense	Homogeneous enhancement	Restricted owing to high cellularity	Type III or IV
Extrarenal rhabdoid tumor	Trunk, mediastinum	Hypo- to isointense	Heterogeneously hyperintense	Heterogeneous and peripheral enhancement due to necrosis	Restricted in solid areas; no restriction in necrotic areas	Type III or IV in solid areas; type I in necrotic areas

Note.—CE = contrast-enhanced, FS = fat-suppressed, MPNST = malignant peripheral nerve sheath tumor, T1W = T1-weighted, T2W = T2-weighted.

Parameningeal rhabdomyosarcoma often manifests as a heterogeneous mass, with solid components alternating with large areas of fluid signal intensity that are hyperintense on T2-weighted images (33). The heterogeneity is secondary to internal necrosis or myxoid component, which correlates with high signal intensity on T2-weighted images and lack of restricted diffusion (34). These tumors need further imaging evaluation of the whole spine to exclude leptomeningeal involvement, although metastases are more frequent in the lung and bone (35).

Paratesticular tumors are isointense to the testicle on T1-weighted images and heterogeneously hyperintense to the testicle on T2-weighted images, with heterogeneous enhancement after contrast material administration (29,36).

Tumors arising in the genitourinary system have the same MRI features on T1- and T2-weighted images as other rhabdomyosarcomas. There is a variable degree of enhancement after intravenous contrast material administration depending on the size of the tumor, as internal vascularization decreases with tumor growth owing to internal necrosis (Fig 5) (37).

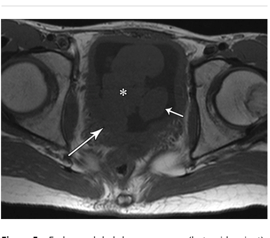

Figure 5a. Embryonal rhabdomyosarcoma (botryoid variant) of the bladder in a 5-year-old girl. **(a)** Axial T1-weighted image shows a multilobulated mass (arrows) arising from the right posterolateral wall of the bladder and protruding into the bladder lumen. The mass (*) is isointense to muscle. **(b)** Axial T2-weighted image shows areas of heterogeneous hypointensity (*) and areas of high signal intensity (arrow) in the lesion, which may represent solid component and necrosis, respectively. **(c)** Axial contrast-enhanced fat-suppressed T1-weighted image shows heterogeneous enhancement of the mass (*) in association with areas that lack enhancement (arrow), which are suggestive of necrosis.

Download as PowerPoint | Open in Image Viewer

Figure 5b. Embryonal rhabdomyosarcoma (botryoid variant) of the bladder in a 5-year-old girl. **(a)** Axial T1-weighted image shows a multilobulated mass (arrows) arising from the right posterolateral wall of the bladder and protruding into the bladder lumen. The mass (*) is isointense to muscle. **(b)** Axial T2-weighted image shows areas of heterogeneous hypointensity (*) and areas of high signal intensity (arrow) in the lesion, which may represent solid component and necrosis, respectively. **(c)** Axial contrast-enhanced fat-suppressed T1-weighted image shows heterogeneous enhancement of the mass (*) in association with areas that lack enhancement (arrow), which are suggestive of necrosis.

Download as PowerPoint | Open in Image Viewer

Figure 5c. Embryonal rhabdomyosarcoma (botryoid variant) of the bladder in a 5-year-old girl. **(a)** Axial T1-weighted image shows a multilobulated mass (arrows) arising from the right posterolateral wall of the bladder and protruding into the bladder lumen. The mass (*) is isointense to muscle. **(b)** Axial T2-weighted image shows areas of heterogeneous hypointensity (*) and areas of high signal intensity (arrow) in the lesion, which may represent solid component and necrosis, respectively. **(c)** Axial contrast-enhanced fat-suppressed T1-weighted image shows heterogeneous enhancement of the mass (*) in association with areas that lack enhancement (arrow), which are suggestive of necrosis.

Download as PowerPoint | Open in Image Viewer

Botryoid rhabdomyosarcoma of the biliary tree may be difficult to distinguish from other hepatic masses—such as hepatoblastoma and undifferentiated embryonal sarcoma—owing to its large size at presentation (37) (Fig 6). The key imaging feature in this sarcoma is origin in and involvement of the biliary tree. At conventional MRI, these tumors are isointense to the liver on T1-weighted images and heterogeneously hyperintense to the liver on T2-weighted images, with central areas of necrosis that appear as heterogeneous areas of high T2 signal intensity with no enhancement after contrast material administration (30).

Figure 6a. Embryonal rhabdomyosarcoma (botryoid variant) of the liver in a 3-year-old boy. **(a)** Axial fat-suppressed T2-weighted image shows a heterogeneously hyperintense liver mass (*) with lobulated margins. The lesion involves and expands the common bile duct (CBD) (white arrow) in association with proximal dilatation of the biliary tree (black arrow). **(b, c)** Axial diffusion-weighted image **(b)** and ADC image **(c)** show restricted diffusion of the mass (*) and of the tumoral component in the CBD (arrow). **(d)** Left: DCE image shows heterogeneous enhancement of the mass (white arrow). The mass also contains areas of necrosis (black arrow). Right: The heterogeneous enhancement correlates with a type III or IV TIC profile (white arrow). The areas of necrosis correlate with a type I curve profile (black arrow). Blue curve = reference standard of arterial uptake.

Download as PowerPoint | Open in Image Viewer

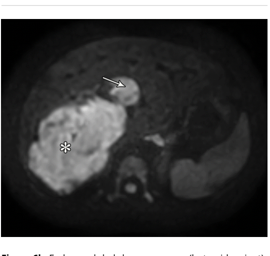

Figure 6b. Embryonal rhabdomyosarcoma (botryoid variant) of the liver in a 3-year-old boy. **(a)** Axial fat-suppressed T2-weighted image shows a heterogeneously hyperintense liver mass (*) with lobulated margins. The lesion involves and expands the common bile duct (CBD) (white arrow) in association with proximal dilatation of the biliary tree (black arrow). **(b, c)** Axial diffusion-weighted image **(b)** and ADC image **(c)** show restricted diffusion of the mass (*) and of the tumoral component in the CBD (arrow). **(d)** Left: DCE image shows heterogeneous enhancement of the mass (white arrow). The mass also contains areas of necrosis (black arrow). Right: The heterogeneous enhancement correlates with a type III or IV TIC profile (white arrow). The areas of necrosis correlate with a type I curve profile (black arrow). Blue curve = reference standard of arterial uptake.

Download as PowerPoint | Open in Image Viewer

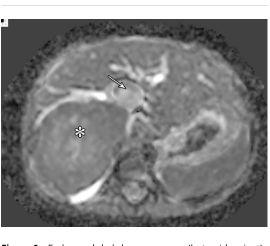

Figure 6c. Embryonal rhabdomyosarcoma (botryoid variant) of the liver in a 3-year-old boy. **(a)** Axial fat-suppressed T2-weighted image shows a heterogeneously hyperintense liver mass (*) with lobulated margins. The lesion involves and expands the common bile duct (CBD) (white arrow) in association with proximal dilatation of the biliary tree (black arrow). **(b, c)** Axial diffusion-weighted image **(b)** and ADC image **(c)** show restricted diffusion of the mass (*) and of the tumoral component in the CBD (arrow). **(d)** Left: DCE image shows heterogeneous enhancement of the mass (white arrow). The mass also contains areas of necrosis (black arrow). Right: The heterogeneous enhancement correlates with a type III or IV TIC profile (white arrow). The areas of necrosis correlate with a type I curve profile (black arrow). Blue curve = reference standard of arterial uptake.

Download as PowerPoint | Open in Image Viewer

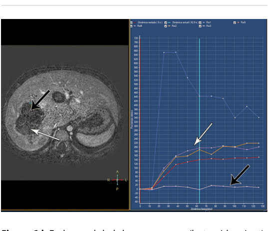

Figure 6d. Embryonal rhabdomyosarcoma (botryoid variant) of the liver in a 3-year-old boy. **(a)** Axial fat-suppressed T2-weighted image shows a heterogeneously hyperintense liver mass (*) with lobulated margins. The lesion involves and expands the common bile duct (CBD) (white arrow) in association with proximal dilatation of the biliary tree (black arrow). **(b, c)** Axial diffusion-weighted image **(b)** and ADC image **(c)** show restricted diffusion of the mass (*) and of the tumoral component in the CBD (arrow). **(d)** Left: DCE image shows heterogeneous enhancement of the mass (white arrow). The mass also contains areas of necrosis (black arrow). Right: The heterogeneous enhancement correlates with a type III or IV TIC profile (white arrow). The areas of necrosis correlate with a type I curve profile (black arrow). Blue curve = reference standard of arterial uptake.

Download as PowerPoint | Open in Image Viewer

***Multiparametric MRI Findings.*—**Owing to its high cellularity, embryonal rhabdomyosarcoma usually shows restricted diffusion, which correlates with low ADC (34). Whole-lesion ADC histogram analysis along with DCE MRI assessment before and after treatment offer a quantitative interpretation of tumor response (19,22).

TICs performed in solid areas correlate with type III and IV curve profiles at DCE MRI, whereas curves performed in areas of hyperintensity on T2-weighted images show a type I curve profile, indicating necrosis or myxoid component (13,18,21,22). After surgery, residual tumor may exhibit type III and IV curve profiles, whereas granulation tissue and fibrosis show type II and V curve profiles.

At DWI, paratesticular tumor does not show restricted diffusion owing to its myxoid component, which correlates with the heterogeneous hyperintensity on T2-weighted images (13,18,34).

Teaching Point Whole-lesion ADC histogram analysis of embryonal rhabdomyosarcoma does not usually demonstrate restriction as a consequence of internal necrosis and myxoid component.

***Treatment.*—**Treatment of embryonal rhabdomyosarcoma depends on the subtype and anatomic location but is mainly based on a combination of chemotherapy drugs. Surgery and radiation therapy may be indicated on a case-by-case basis, depending on tumor location and stage (38). This plan has been proposed by the Children's Oncology Group (COG) in the United States and the more recently founded European Pediatric Soft Tissue Sarcoma Study Group (EpSSG) in Europe (5,38). The reported 5-year survival rate exceeds 70% for patients with localized rhabdomyosarcoma (38).

Alveolar Rhabdomyosarcoma

***Epidemiologic Features.*—**Alveolar rhabdomyosarcoma represents 15%–20% of all rhabdomyosarcomas and is more common in older children and young adults, typically between 10 and 25 years of age (24).

***Clinical Features.*—**Alveolar rhabdomyosarcoma manifests as a painless mass of indolent growth, as it usually arises in the deep soft tissues of the extremities and trunk (23,32).

***Histopathologic Findings.*—**Alveolar rhabdomyosarcoma is a highly cellular tumor with fibrous stroma and fibrovascular septa that tends to peripheral discohesion with an alveoli-like appearance. The expression of myogenin is typically stronger and more diffuse than in embryonal rhabdomyosarcoma (39). Alveolar rhabdomyosarcoma has consistent translocations, resulting in fusion of a transcription factor with the genes *PAX3* or *PAX7*.

There is a well-established algorithm protocol for histopathologic diagnosis of alveolar rhabdomyosarcoma, which includes a multidisciplinary team of radiologists, pathologists, and molecular biologists (Fig 7) (40).

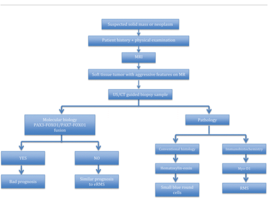

Figure 7. Algorithm for histopathologic diagnosis of alveolar rhabdomyosarcoma *(RMS)*. *eRMS* = embryonal rhabdomyosarcoma.

Download as PowerPoint | Open in Image Viewer

***Conventional MRI Findings.*—**Findings are similar to those in other soft-tissue sarcomas, with the lesion being iso- to hyperintense to muscle on T1-weighted images and heterogeneously hyperintense to muscle on T2-weighted images (Fig 8) (41,42). Involvement of adjacent bone with erosions or subperiosteal new bone formation is found in approximately 25% of patients (6,42). Alveolar rhabdomyosarcoma typically shows muscle and fascial involvement.

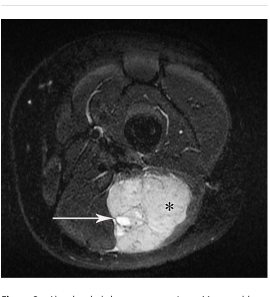

Figure 8a. Alveolar rhabdomyosarcoma in an 11-year-old boy with a left thigh mass. **(a)** Axial fat-suppressed T2-weighted image shows a lobulated heterogeneously hyperintense lesion (*) with a peripheral cystic or necrotic component (arrow) involving the biceps femoris muscle. **(b)** DCE image shows diffuse early enhancement of the tumor (black arrow). This finding correlates with a type III or IV TIC profile (white arrow). Blue curve = reference standard of arterial uptake. **(c)** Axial diffusion-weighted image and ADC image show restricted diffusion in the mass (*). **(d)** Axial contrast-enhanced fat-suppressed T1-weighted image after chemotherapy shows significant shrinkage of the tumor (*), with persistence of heterogeneous enhancement. **(e)** Graphs from volumetric determination of ADC show ADC of 0.78 × 10^{-3} mm^2/sec with a high and sharp ADC histogram before treatment (white arrow). ADC after 2 months of treatment was 1.06 × 10^{-3} mm^2/sec with a short and wide ADC histogram with rightward shift (black arrow). There was 50% reduction of tumor volume in the interval.

Download as PowerPoint | Open in Image Viewer

Figure 8b. Alveolar rhabdomyosarcoma in an 11-year-old boy with a left thigh mass. **(a)** Axial fat-suppressed T2-weighted image shows a lobulated heterogeneously hyperintense lesion (*) with a peripheral cystic or necrotic component (arrow) involving the biceps femoris muscle. **(b)** DCE image shows diffuse early enhancement of the tumor (black arrow). This finding correlates with a type III or IV TIC profile (white arrow). Blue curve = reference standard of arterial uptake. **(c)** Axial diffusion-weighted image and ADC image show restricted diffusion in the mass (*). **(d)** Axial contrast-enhanced fat-suppressed T1-weighted image after chemotherapy shows significant shrinkage of the tumor (*), with persistence of heterogeneous enhancement. **(e)** Graphs from volumetric determination of ADC show ADC of 0.78 × 10^{-3} mm^2/sec with a high and sharp ADC histogram before treatment (white arrow). ADC after 2 months of treatment was 1.06 × 10^{-3} mm^2/sec with a short and wide ADC histogram with rightward shift (black arrow). There was 50% reduction of tumor volume in the interval.

Download as PowerPoint | Open in Image Viewer

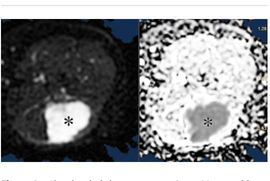

Figure 8c. Alveolar rhabdomyosarcoma in an 11-year-old boy with a left thigh mass. **(a)** Axial fat-suppressed T2-weighted image shows a lobulated heterogeneously hyperintense lesion (*) with a peripheral cystic or necrotic component (arrow) involving the biceps femoris muscle. **(b)** DCE image shows diffuse early enhancement of the tumor (black arrow). This finding correlates with a type III or IV TIC profile (white arrow). Blue curve = reference standard of arterial uptake. **(c)** Axial diffusion-weighted image and ADC image show restricted diffusion in the mass (*). **(d)** Axial contrast-enhanced fat-suppressed T1-weighted image after chemotherapy shows significant shrinkage of the tumor (*), with persistence of heterogeneous enhancement. **(e)** Graphs from volumetric determination of ADC show ADC of 0.78 × 10^{-3} mm^2/sec with a high and sharp ADC histogram before treatment (white arrow). ADC after 2 months of treatment was 1.06 × 10^{-3} mm^2/sec with a short and wide ADC histogram with rightward shift (black arrow). There was 50% reduction of tumor volume in the interval.

Download as PowerPoint | Open in Image Viewer

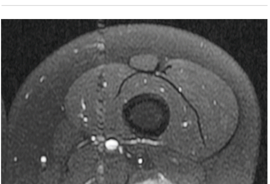

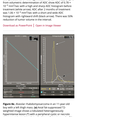

Figure 1a. Alveolar rhabdomyosarcoma in a 1-year-old boy with 2-year history of a progressively enlarged mass in the thigh. Axial T1-weighted image after contrast enhancement demonstrates a heterogenously enhancing mass with areas of necrosis (arrowhead). Note the presence of enlarged inguinal lymph nodes (arrows). This finding is consistent with a stage III or IV tumor. **(b)** Coronal T2-weighted image with fat suppression. Note the diffuse edema and the presence of a large amount of fluid in the tissues of the thigh. This finding is consistent with an unfavorable histologic subtype. **(c)** Coronal T1-weighted image after contrast enhancement with fat suppression. Note the presence of enhancement in the tissues of the thigh. This finding is consistent with presence of tumor. **(d)** Coronal T1-weighted image after contrast enhancement with fat suppression. Note the presence of enhancement in the tissues of the thigh. This finding is consistent with presence of tumor. **(e)** Coronal T1-weighted image after contrast enhancement with fat suppression. Note the presence of enhancement in the tissues of the thigh. This finding is consistent with presence of tumor. **(f)** Coronal T1-weighted image after contrast enhancement with fat suppression. Note the presence of enhancement in the tissues of the thigh. This finding is consistent with presence of tumor.

Figure 1b. Alveolar rhabdomyosarcoma in 1-year-old boy with 2-year history of a progressively enlarged mass in the thigh. Axial T1-weighted image after contrast enhancement demonstrates a heterogenously enhancing mass with areas of necrosis (arrowhead). Note the presence of enlarged inguinal lymph nodes (arrows). This finding is consistent with a stage III or IV tumor. **(b)** Coronal T2-weighted image with fat suppression. Note the diffuse edema and the presence of a large amount of fluid in the tissues of the thigh. This finding is consistent with an unfavorable histologic subtype. **(c)** Coronal T1-weighted image after contrast enhancement with fat suppression. Note the presence of enhancement in the tissues of the thigh. This finding is consistent with presence of tumor. **(d)** Coronal T1-weighted image after contrast enhancement with fat suppression. Note the presence of enhancement in the tissues of the thigh. This finding is consistent with presence of tumor. **(e)** Coronal T1-weighted image after contrast enhancement with fat suppression. Note the presence of enhancement in the tissues of the thigh. This finding is consistent with presence of tumor. **(f)** Coronal T1-weighted image after contrast enhancement with fat suppression. Note the presence of enhancement in the tissues of the thigh. This finding is consistent with presence of tumor.

Treatment—The survival of children with rhabdomyosarcoma has improved significantly with the advent of multimodal therapy. Treatment options for rhabdomyosarcoma include chemotherapy, drug with surgery and in some instances radiation therapy. The Intergroup Rhabdomyosarcoma Study Group (IRSG) has established risk-based treatment protocols.

The pediatric type has the worst prognosis among all rhabdomyosarcomas. Children with alveolar rhabdomyosarcoma have a worse prognosis if compared with those with other histologic subtypes of the disease (survival, most frequently in the bone, lung, or bone marrow). The presence of metastatic disease is the most ominous sign.

The differential diagnosis of rhabdomyosarcoma is broad and includes other soft tissue tumors and inflammatory processes. Imaging plays an important role in the diagnosis, staging, and evaluation of response to therapy. Rhabdomyosarcoma is the most common soft tissue sarcoma in children, depending on the location, and can of IRSG With the exception of the orbital and genitourinary (GU) tumors, the prognosis for children with rhabdomyosarcoma is poor. Survival is dependent on the stage of the disease.

Malignant Peripheral Nerve Sheath Tumor

Epidemiologic Features—MPNST is a rare malignant tumor, accounting for approximately 5% of all soft tissue sarcomas. Approximately 50% of MPNST occur in patients with neurofibromatosis. Most commonly hypointense areas within the tumor, which correspond to areas of fibrosis or myxoid degeneration. Note the involvement of the adjacent soft tissue and bone. **(b)** Axial contrast-enhanced fat-suppressed T1-weighted image shows minimal peripheral enhancement. Note the presence of a large amount of fluid in the tissues of the thigh. This finding is consistent with presence of the tumor. **(c)** Axial T2-weighted image with fat suppression. Note the presence of a large amount of fluid in the tissues of the thigh. This finding is consistent with presence of the tumor. **(d)** Axial T2-weighted image with fat suppression. Note the presence of a large amount of fluid in the tissues of the thigh. This finding is consistent with presence of the tumor. **(e)** Axial T2-weighted image with fat suppression. Note the presence of a large amount of fluid in the tissues of the thigh. This finding is consistent with presence of the tumor. **(f)** Axial T2-weighted image with fat suppression. Note the presence of a large amount of fluid in the tissues of the thigh. This finding is consistent with presence of the tumor.

Figure 2a. Axial T1-weighted image with fat suppression. Note the presence of a large amount of fluid in the tissues of the thigh. This finding is consistent with presence of the tumor. **(b)** Axial T2-weighted image with fat suppression. Note the presence of a large amount of fluid in the tissues of the thigh. This finding is consistent with presence of the tumor. **(c)** Axial T2-weighted image with fat suppression. Note the presence of a large amount of fluid in the tissues of the thigh. This finding is consistent with presence of the tumor. **(d)** Axial T2-weighted image with fat suppression. Note the presence of a large amount of fluid in the tissues of the thigh. This finding is consistent with presence of the tumor. **(e)** Axial T2-weighted image with fat suppression. Note the presence of a large amount of fluid in the tissues of the thigh. This finding is consistent with presence of the tumor. **(f)** Axial T2-weighted image with fat suppression. Note the presence of a large amount of fluid in the tissues of the thigh. This finding is consistent with presence of the tumor.

Treatment—The survival of children with rhabdomyosarcoma has improved significantly with the advent of multimodal therapy. Treatment options for rhabdomyosarcoma include chemotherapy, drug with surgery and in some instances radiation therapy. The Intergroup Rhabdomyosarcoma Study Group (IRSG) has established risk-based treatment protocols.

The pediatric type has the worst prognosis among all rhabdomyosarcomas. Children with alveolar rhabdomyosarcoma have a worse prognosis if compared with those with other histologic subtypes of the disease (survival, most frequently in the bone, lung, or bone marrow). The presence of metastatic disease is the most ominous sign.

The differential diagnosis of rhabdomyosarcoma is broad and includes other soft tissue tumors and inflammatory processes. Imaging plays an important role in the diagnosis, staging, and evaluation of response to therapy. Rhabdomyosarcoma is the most common soft tissue sarcoma in children, depending on the location, and can of IRSG With the exception of the orbital and genitourinary (GU) tumors, the prognosis for children with rhabdomyosarcoma is poor. Survival is dependent on the stage of the disease.

Malignant Peripheral Nerve Sheath Tumor

Epidemiologic Features—MPNST is a rare malignant tumor, accounting for approximately 5% of all soft tissue sarcomas. Approximately 50% of MPNST occur in patients with neurofibromatosis. Most commonly hypointense areas within the tumor, which correspond to areas of fibrosis or myxoid degeneration. Note the involvement of the adjacent soft tissue and bone. **(b)** Axial contrast-enhanced fat-suppressed T1-weighted image shows minimal peripheral enhancement. Note the presence of a large amount of fluid in the tissues of the thigh. This finding is consistent with presence of the tumor. **(c)** Axial T2-weighted image with fat suppression. Note the presence of a large amount of fluid in the tissues of the thigh. This finding is consistent with presence of the tumor. **(d)** Axial T2-weighted image with fat suppression. Note the presence of a large amount of fluid in the tissues of the thigh. This finding is consistent with presence of the tumor. **(e)** Axial T2-weighted image with fat suppression. Note the presence of a large amount of fluid in the tissues of the thigh. This finding is consistent with presence of the tumor. **(f)** Axial T2-weighted image with fat suppression. Note the presence of a large amount of fluid in the tissues of the thigh. This finding is consistent with presence of the tumor.

Figure 2b. MPNST in a 14-year-old boy with NF1. **(a)** Axial T1-weighted image shows a multilobulated mass with areas of necrosis (arrowhead). Note the involvement of the adjacent soft tissue and bone. **(b)** Axial contrast-enhanced fat-suppressed T1-weighted image shows minimal peripheral enhancement. Note the presence of a large amount of fluid in the tissues of the thigh. This finding is consistent with presence of the tumor. **(c)** Axial T2-weighted image with fat suppression. Note the presence of a large amount of fluid in the tissues of the thigh. This finding is consistent with presence of the tumor. **(d)** Axial T2-weighted image with fat suppression. Note the presence of a large amount of fluid in the tissues of the thigh. This finding is consistent with presence of the tumor. **(e)** Axial T2-weighted image with fat suppression. Note the presence of a large amount of fluid in the tissues of the thigh. This finding is consistent with presence of the tumor. **(f)** Axial T2-weighted image with fat suppression. Note the presence of a large amount of fluid in the tissues of the thigh. This finding is consistent with presence of the tumor.

Figure 2c. MPNST in a 14-year-old boy with NF1. **(a)** Axial T1-weighted image shows a multilobulated mass with areas of necrosis (arrowhead). Note the involvement of the adjacent soft tissue and bone. **(b)** Axial contrast-enhanced fat-suppressed T1-weighted image shows minimal peripheral enhancement. Note the presence of a large amount of fluid in the tissues of the thigh. This finding is consistent with presence of the tumor. **(c)** Axial T2-weighted image with fat suppression. Note the presence of a large amount of fluid in the tissues of the thigh. This finding is consistent with presence of the tumor. **(d)** Axial T2-weighted image with fat suppression. Note the presence of a large amount of fluid in the tissues of the thigh. This finding is consistent with presence of the tumor. **(e)** Axial T2-weighted image with fat suppression. Note the presence of a large amount of fluid in the tissues of the thigh. This finding is consistent with presence of the tumor. **(f)** Axial T2-weighted image with fat suppression. Note the presence of a large amount of fluid in the tissues of the thigh. This finding is consistent with presence of the tumor.

Figure 2d. MPNST in a 14-year-old boy with NF1. **(a)** Axial T1-weighted image shows a multilobulated mass with areas of necrosis (arrowhead). Note the involvement of the adjacent soft tissue and bone. **(b)** Axial contrast-enhanced fat-suppressed T1-weighted image shows minimal peripheral enhancement. Note the presence of a large amount of fluid in the tissues of the thigh. This finding is consistent with presence of the tumor. **(c)** Axial T2-weighted image with fat suppression. Note the presence of a large amount of fluid in the tissues of the thigh. This finding is consistent with presence of the tumor. **(d)** Axial T2-weighted image with fat suppression. Note the presence of a large amount of fluid in the tissues of the thigh. This finding is consistent with presence of the tumor. **(e)** Axial T2-weighted image with fat suppression. Note the presence of a large amount of fluid in the tissues of the thigh. This finding is consistent with presence of the tumor. **(f)** Axial T2-weighted image with fat suppression. Note the presence of a large amount of fluid in the tissues of the thigh. This finding is consistent with presence of the tumor.

Figure 2e. MPNST in a 14-year-old boy with NF1. **(a)** Axial T1-weighted image shows a multilobulated mass with areas of necrosis (arrowhead). Note the involvement of the adjacent soft tissue and bone. **(b)** Axial contrast-enhanced fat-suppressed T1-weighted image shows minimal peripheral enhancement. Note the presence of a large amount of fluid in the tissues of the thigh. This finding is consistent with presence of the tumor. **(c)** Axial T2-weighted image with fat suppression. Note the presence of a large amount of fluid in the tissues of the thigh. This finding is consistent with presence of the tumor. **(d)** Axial T2-weighted image with fat suppression. Note the presence of a large amount of fluid in the tissues of the thigh. This finding is consistent with presence of the tumor. **(e)** Axial T2-weighted image with fat suppression. Note the presence of a large amount of fluid in the tissues of the thigh. This finding is consistent with presence of the tumor. **(f)** Axial T2-weighted image with fat suppression. Note the presence of a large amount of fluid in the tissues of the thigh. This finding is consistent with presence of the tumor.

Figure 2f. MPNST in a 14-year-old boy with NF1. **(a)** Axial T1-weighted image shows a multilobulated mass with areas of necrosis (arrowhead). Note the involvement of the adjacent soft tissue and bone. **(b)** Axial contrast-enhanced fat-suppressed T1-weighted image shows minimal peripheral enhancement. Note the presence of a large amount of fluid in the tissues of the thigh. This finding is consistent with presence of the tumor. **(c)** Axial T2-weighted image with fat suppression. Note the presence of a large amount of fluid in the tissues of the thigh. This finding is consistent with presence of the tumor. **(d)** Axial T2-weighted image with fat suppression. Note the presence of a large amount of fluid in the tissues of the thigh. This finding is consistent with presence of the tumor. **(e)** Axial T2-weighted image with fat suppression. Note the presence of a large amount of fluid in the tissues of the thigh. This finding is consistent with presence of the tumor. **(f)** Axial T2-weighted image with fat suppression. Note the presence of a large amount of fluid in the tissues of the thigh. This finding is consistent with presence of the tumor.

Figure 2g. MPNST in a 14-year-old boy with NF1. **(a)** Axial T1-weighted image shows a multilobulated mass with areas of necrosis (arrowhead). Note the involvement of the adjacent soft tissue and bone. **(b)** Axial contrast-enhanced fat-suppressed T1-weighted image shows minimal peripheral enhancement. Note the presence of a large amount of fluid in the tissues of the thigh. This finding is consistent with presence of the tumor. **(c)** Axial T2-weighted image with fat suppression. Note the presence of a large amount of fluid in the tissues of the thigh. This finding is consistent with presence of the tumor. **(d)** Axial T2-weighted image with fat suppression. Note the presence of a large amount of fluid in the tissues of the thigh. This finding is consistent with presence of the tumor. **(e)** Axial T2-weighted image with fat suppression. Note the presence of a large amount of fluid in the tissues of the thigh. This finding is consistent with presence of the tumor. **(f)** Axial T2-weighted image with fat suppression. Note the presence of a large amount of fluid in the tissues of the thigh. This finding is consistent with presence of the tumor.

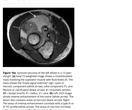

Figure 2h. MPNST in a 14-year-old boy with NF1. **(a)** Axial T1-weighted image shows a multilobulated mass with areas of necrosis (arrowhead). Note the involvement of the adjacent soft tissue and bone. **(b)** Axial contrast-enhanced fat-suppressed T1-weighted image shows minimal peripheral enhancement. Note the presence of a large amount of fluid in the tissues of the thigh. This finding is consistent with presence of the tumor. **(c)** Axial T2-weighted image with fat suppression. Note the presence of a large amount of fluid in the tissues of the thigh. This finding is consistent with presence of the tumor. **(d)** Axial T2-weighted image with fat suppression. Note the presence of a large amount of fluid in the tissues of the thigh. This finding is consistent with presence of the tumor. **(e)** Axial T2-weighted image with fat suppression. Note the presence of a large amount of fluid in the tissues of the thigh. This finding is consistent with presence of the tumor. **(f)** Axial T2-weighted image with fat suppression. Note the presence of a large amount of fluid in the tissues of the thigh. This finding is consistent with presence of the tumor.

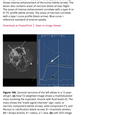

Figure 2i. MPNST in a 14-year-old boy with NF1. **(a)** Axial T1-weighted image shows a multilobulated mass with areas of necrosis (arrowhead). Note the involvement of the adjacent soft tissue and bone. **(b)** Axial contrast-enhanced fat-suppressed T1-weighted image shows minimal peripheral enhancement. Note the presence of a large amount of fluid in the tissues of the thigh. This finding is consistent with presence of the tumor. **(c)** Axial T2-weighted image with fat suppression. Note the presence of a large amount of fluid in the tissues of the thigh. This finding is consistent with presence of the tumor. **(d)** Axial T2-weighted image with fat suppression. Note the presence of a large amount of fluid in the tissues of the thigh. This finding is consistent with presence of the tumor. **(e)** Axial T2-weighted image with fat suppression. Note the presence of a large amount of fluid in the tissues of the thigh. This finding is consistent with presence of the tumor. **(f)** Axial T2-weighted image with fat suppression. Note the presence of a large amount of fluid in the tissues of the thigh. This finding is consistent with presence of the tumor.

Figure 2j. MPNST in a 14-year-old boy with NF1. **(a)** Axial T1-weighted image shows a multilobulated mass with areas of necrosis (arrowhead). Note the involvement of the adjacent soft tissue and bone. **(b)** Axial contrast-enhanced fat-suppressed T1-weighted image shows minimal peripheral enhancement. Note the presence of a large amount of fluid in the tissues of the thigh. This finding is consistent with presence of the tumor. **(c)** Axial T2-weighted image with fat suppression. Note the presence of a large amount of fluid in the tissues of the thigh. This finding is consistent with presence of the tumor. **(d)** Axial T2-weighted image with fat suppression. Note the presence of a large amount of fluid in the tissues of the thigh. This finding is consistent with presence of the tumor. **(e)** Axial T2-weighted image with fat suppression. Note the presence of a large amount of fluid in the tissues of the thigh. This finding is consistent with presence of the tumor. **(f)** Axial T2-weighted image with fat suppression. Note the presence of a large amount of fluid in the tissues of the thigh. This finding is consistent with presence of the tumor.

Figure 2k. MPNST in a 14-year-old boy with NF1. **(a)** Axial T1-weighted image shows a multilobulated mass with areas of necrosis (arrowhead). Note the involvement of the adjacent soft tissue and bone. **(b)** Axial contrast-enhanced fat-suppressed T1-weighted image shows minimal peripheral enhancement. Note the presence of a large amount of fluid in the tissues of the thigh. This finding is consistent with presence of the tumor. **(c)** Axial T2-weighted image with fat suppression. Note the presence of a large amount of fluid in the tissues of the thigh. This finding is consistent with presence of the tumor. **(d)** Axial T2-weighted image with fat suppression. Note the presence of a large amount of fluid in the tissues of the thigh. This finding is consistent with presence of the tumor. **(e)** Axial T2-weighted image with fat suppression. Note the presence of a large amount of fluid in the tissues of the thigh. This finding is consistent with presence of the tumor. **(f)** Axial T2-weighted image with fat suppression. Note the presence of a large amount of fluid in the tissues of the thigh. This finding is consistent with presence of the tumor.

Figure 2l. MPNST in a 14-year-old boy with NF1. **(a)** Axial T1-weighted image shows a multilobulated mass with areas of necrosis (arrowhead). Note the involvement of the adjacent soft tissue and bone. **(b)** Axial contrast-enhanced fat-suppressed T1-weighted image shows minimal peripheral enhancement. Note the presence of a large amount of fluid in the tissues of the thigh. This finding is consistent with presence of the tumor. **(c)** Axial T2-weighted image with fat suppression. Note the presence of a large amount of fluid in the tissues of the thigh. This finding is consistent with presence of the tumor. **(d)** Axial T2-weighted image with fat suppression. Note the presence of a large amount of fluid in the tissues of the thigh. This finding is consistent with presence of the tumor. **(e)** Axial T2-weighted image with fat suppression. Note the presence of a large amount of fluid in the tissues of the thigh. This finding is consistent with presence of the tumor. **(f)** Axial T2-weighted image with fat suppression. Note the presence of a large amount of fluid in the tissues of the thigh. This finding is consistent with presence of the tumor.

Figure 2m. MPNST in a 14-year-old boy with NF1. **(a)** Axial T1-weighted image shows a multilobulated mass with areas of necrosis (arrowhead). Note the involvement of the adjacent soft tissue and bone. **(b)** Axial contrast-enhanced fat-suppressed T1-weighted image shows minimal peripheral enhancement. Note the presence of a large amount of fluid in the tissues of the thigh. This finding is consistent with presence of the tumor. **(c)** Axial T2-weighted image with fat suppression. Note the presence of a large amount of fluid in the tissues of the thigh. This finding is consistent with presence of the tumor. **(d)** Axial T2-weighted image with fat suppression. Note the presence of a large amount of fluid in the tissues of the thigh. This finding is consistent with presence of the tumor. **(e)** Axial T2-weighted image with fat suppression. Note the presence of a large amount of fluid in the tissues of the thigh. This finding is consistent with presence of the tumor. **(f)** Axial T2-weighted image with fat suppression. Note the presence of a large amount of fluid in the tissues of the thigh. This finding is consistent with presence of the tumor.

Figure 2n. MPNST in a 14-year-old boy with NF1. **(a)** Axial T1-weighted image shows a multilobulated mass with areas of necrosis (arrowhead). Note the involvement of the adjacent soft tissue and bone. **(b)** Axial contrast-enhanced fat-suppressed T1-weighted image shows minimal peripheral enhancement. Note the presence of a large amount of fluid in the tissues of the thigh. This finding is consistent with presence of the tumor. **(c)** Axial T2-weighted image with fat suppression. Note the presence of a large amount of fluid in the tissues of the thigh. This finding is consistent with presence of the tumor. **(d)** Axial T2-weighted image with fat suppression. Note the presence of a large amount of fluid in the tissues of the thigh. This finding is consistent with presence of the tumor. **(e)** Axial T2-weighted image with fat suppression. Note the presence of a large amount of fluid in the tissues of the thigh. This finding is consistent with presence of the tumor. **(f)** Axial T2-weighted image with fat suppression. Note the presence of a large amount of fluid in the tissues of the thigh. This finding is consistent with presence of the tumor.

Figure 2o. MPNST in a 14-year-old boy with NF1. **(a)** Axial T1-weighted image shows a multilobulated mass with areas of necrosis (arrowhead). Note the involvement of the adjacent soft tissue and bone. **(b)** Axial contrast-enhanced fat-suppressed T1-weighted image shows minimal peripheral enhancement. Note the presence of a large amount of fluid in the tissues of the thigh. This finding is consistent with presence of the tumor. **(c)** Axial T2-weighted image with fat suppression. Note the presence of a large amount of fluid in the tissues of the thigh. This finding is consistent with presence of the tumor. **(d)** Axial T2-weighted image with fat suppression. Note the presence of a large amount of fluid in the tissues of the thigh. This finding is consistent with presence of the tumor. **(e)** Axial T2-weighted image with fat suppression. Note the presence of a large amount of fluid in the tissues of the thigh. This finding is consistent with presence of the tumor. **(f)** Axial T2-weighted image with fat suppression. Note the presence of a large amount of fluid in the tissues of the thigh. This finding is consistent with presence of the tumor.

Figure 2p. MPNST in a 14-year-old boy with NF1. **(a)** Axial T1-weighted image shows a multilobulated mass with areas of necrosis (arrowhead). Note the involvement of the adjacent soft tissue and bone. **(b)** Axial contrast-enhanced fat-suppressed T1-weighted image shows minimal peripheral enhancement. Note the presence of a large amount of fluid in the tissues of the thigh. This finding is consistent with presence of the tumor. **(c)** Axial T2-weighted image with fat suppression. Note the presence of a large amount of fluid in the tissues of the thigh. This finding is consistent with presence of the tumor. **(d)** Axial T2-weighted image with fat suppression. Note the presence of a large amount of fluid in the tissues of the thigh. This finding is consistent with presence of the tumor. **(e)** Axial T2-weighted image with fat suppression. Note the presence of a large amount of fluid in the tissues of the thigh. This finding is consistent with presence of the tumor. **(f)** Axial T2-weighted image with fat suppression. Note the presence of a large amount of fluid in the tissues of the thigh. This finding is consistent with presence of the tumor.

Figure 2q. MPNST in a 14-year-old boy with NF1. **(a)** Axial T1-weighted image shows a multilobulated mass with areas of necrosis (arrowhead). Note the involvement of the adjacent soft tissue and bone. **(b)** Axial contrast-enhanced fat-suppressed T1-weighted image shows minimal peripheral enhancement. Note the presence of a large amount of fluid in the tissues of the thigh. This finding is consistent with presence of the tumor. **(c)** Axial T2-weighted image with fat suppression. Note the presence of a large amount of fluid in the tissues of the thigh. This finding is consistent with presence of the tumor. **(d)** Axial T2-weighted image with fat suppression. Note the presence of a large amount of fluid in the tissues of the thigh. This finding is consistent with presence of the tumor. **(e)** Axial T2-weighted image with fat suppression. Note the presence of a large amount of fluid in the tissues of the thigh. This finding is consistent with presence of the tumor. **(f)** Axial T2-weighted image with fat suppression. Note the presence of a large amount of fluid in the tissues of the thigh. This finding is consistent with presence of the tumor.

Figure 2r. MPNST in a 14-year-old boy with NF1. **(a)** Axial T1-weighted image shows a multilobulated mass with areas of necrosis (arrowhead). Note the involvement of the adjacent soft tissue and bone. **(b)** Axial contrast-enhanced fat-suppressed T1-weighted image shows minimal peripheral enhancement. Note the presence of a large amount of fluid in the tissues of the thigh. This finding is consistent with presence of the tumor. **(c)** Axial T2-weighted image with fat suppression. Note the presence of a large amount of fluid in the tissues of the thigh. This finding is consistent with presence of the tumor. **(d)** Axial T2-weighted image with fat suppression. Note the presence of a large amount of fluid in the tissues of the thigh. This finding is consistent with presence of the tumor. **(e)** Axial T2-weighted image with fat suppression. Note the presence of a large amount of fluid in the tissues of the thigh. This finding is consistent with presence of the tumor. **(f)** Axial T2-weighted image with fat suppression. Note the presence of a large amount of fluid in the tissues of the thigh. This finding is consistent with presence of the tumor.

Figure 2s. MPNST in a 14-year-old boy with NF1. **(a)** Axial T1-weighted image shows a multilobulated mass with areas of necrosis (arrowhead). Note the involvement of the adjacent soft tissue and bone. **(b)** Axial contrast-enhanced fat-suppressed T1-weighted image shows minimal peripheral enhancement. Note the presence of a large amount of fluid in the tissues of the thigh. This finding is consistent with presence of the tumor. **(c)** Axial T2-weighted image with fat suppression. Note the presence of a large amount of fluid in the tissues of the thigh. This finding is consistent with presence of the tumor. **(d)** Axial T2-weighted image with fat suppression. Note the presence of a large amount of fluid in the tissues of the thigh. This finding is consistent with presence of the tumor. **(e)** Axial T2-weighted image with fat suppression. Note the presence of a large amount of fluid in the tissues of the thigh. This finding is consistent with presence of the tumor. **(f)** Axial T2-weighted image with fat suppression. Note the presence of a large amount of fluid in the tissues of the thigh. This finding is consistent with presence of the tumor.

Figure 2t. MPNST in a 14-year-old boy with NF1. **(a)** Axial T1-weighted image shows a multilobulated mass with areas of necrosis (arrowhead). Note the involvement of the adjacent soft tissue and bone. **(b)** Axial contrast-enhanced fat-suppressed T1-weighted image shows minimal peripheral enhancement. Note the presence of a large amount of fluid in the tissues of the thigh. This finding is consistent with presence of the tumor. **(c)** Axial T2-weighted image with fat suppression. Note the presence of a large amount of fluid in the tissues of the thigh. This finding is consistent with presence of the tumor. **(d)** Axial T2-weighted image with fat suppression. Note the presence of a large amount of fluid in the tissues of the thigh. This finding is consistent with presence of the tumor. **(e)** Axial T2-weighted image with fat suppression. Note the presence of a large amount of fluid in the tissues of the thigh. This finding is consistent with presence of the tumor. **(f)** Axial T2-weighted image with fat suppression. Note the presence of a large amount of fluid in the tissues of the thigh. This finding is consistent with presence of the tumor.

Figure 2u. MPNST in a 14-year-old boy with NF1. **(a)** Axial T1-weighted image shows a multilobulated mass with areas of necrosis (arrowhead). Note the involvement of the adjacent soft tissue and bone. **(b)** Axial contrast-enhanced fat-suppressed T1-weighted image shows minimal peripheral enhancement. Note the presence of a large amount of fluid in the tissues of the thigh. This finding is consistent with presence of the tumor. **(c)** Axial T2-weighted image with fat suppression. Note the presence of a large amount of fluid in the tissues of the thigh. This finding is consistent with presence of the tumor. **(d)** Axial T2-weighted image with fat suppression. Note the presence of a large amount of fluid in the tissues of the thigh. This finding is consistent with presence of the tumor. **(e)** Axial T2-weighted image with fat suppression. Note the presence of a large amount of fluid in the tissues of the thigh. This finding is consistent with presence of the tumor. **(f)** Axial T2-weighted image with fat suppression. Note the presence of a large amount of fluid in the tissues of the thigh. This finding is consistent with presence of the tumor.

Figure 2v. MPNST in a 14-year-old boy with NF1. **(a)** Axial T1-weighted image shows a multilobulated mass with areas of necrosis (arrowhead). Note the involvement of the adjacent soft tissue and bone. **(b)** Axial contrast-enhanced fat-suppressed T1-weighted image shows minimal peripheral enhancement. Note the presence of a large amount of fluid in the tissues of the thigh. This finding is consistent with presence of the tumor. **(c)** Axial T2-weighted image with fat suppression. Note the presence of a large amount of fluid in the tissues of the thigh. This finding is consistent with presence of the tumor. **(d)** Axial T2-weighted image with fat suppression. Note the presence of a large amount of fluid in the tissues of the thigh. This finding is consistent with presence of the tumor. **(e)** Axial T2-weighted image with fat suppression. Note the presence of a large amount of fluid in the tissues of the thigh. This finding is consistent with presence of the tumor. **(f)** Axial T2-weighted image with fat suppression. Note the presence of a large amount of fluid in the tissues of the thigh. This finding is consistent with presence of the tumor.

Figure 3a. Congenital fibromatosis of the left foot in a 1-year-old girl. **(a)** Long-axis T1-weighted T2-weighted image shows a large soft tissue mass involving the medial aspect of the foot, with involvement of the adjacent bone. **(b)** Long-axis T1-weighted image after contrast enhancement shows heterogeneous enhancement of the mass. **(c)** Short-axis contrast-enhanced fat-suppressed T1-weighted image shows heterogeneous enhancement of the mass. **(d)** Short-axis T2-weighted image with fat suppression shows heterogeneous signal intensity of the mass. **(e)** Short-axis T2-weighted image with fat suppression shows heterogeneous signal intensity of the mass. **(f)** Short-axis contrast-enhanced fat-suppressed T1-weighted image shows heterogeneous enhancement of the mass.

Figure 3b. Congenital fibromatosis of the left foot in a 1-year-old girl. **(a)** Long-axis T1-weighted T2-weighted image shows a large soft tissue mass involving the medial aspect of the foot, with involvement of the adjacent bone. **(b)** Long-axis T1-weighted image after contrast enhancement shows heterogeneous enhancement of the mass. **(c)** Short-axis contrast-enhanced fat-suppressed T1-weighted image shows heterogeneous enhancement of the mass. **(d)** Short-axis T2-weighted image with fat suppression shows heterogeneous signal intensity of the mass. **(e)** Short-axis T2-weighted image with fat suppression shows heterogeneous signal intensity of the mass. **(f)** Short-axis contrast-enhanced fat-suppressed T1-weighted image shows heterogeneous enhancement of the mass.

Figure 3c. Congenital fibromatosis of the left foot in a 1-year-old girl. **(a)** Long-axis T1-weighted T2-weighted image shows a large soft tissue mass involving the medial aspect of the foot, with involvement of the adjacent bone. **(b)** Long-axis T1-weighted image after contrast enhancement shows heterogeneous enhancement of the mass. **(c)** Short-axis contrast-enhanced fat-suppressed T1-weighted image shows heterogeneous enhancement of the mass. **(d)** Short-axis T2-weighted image with fat suppression shows heterogeneous signal intensity of the mass. **(e)** Short-axis T2-weighted image with fat suppression shows heterogeneous signal intensity of the mass. **(f)** Short-axis contrast-enhanced fat-suppressed T1-weighted image shows heterogeneous enhancement of the mass.

Figure 3d. Congenital fibromatosis of the left foot in a 1-year-old girl. **(a)** Long-axis T1-weighted T2-weighted image shows a large soft tissue mass involving the medial aspect of the foot, with involvement of the adjacent bone. **(b)** Long-axis T1-weighted image after contrast enhancement shows heterogeneous enhancement of the mass. **(c)** Short-axis contrast-enhanced fat-suppressed T1-weighted image shows heterogeneous enhancement of the mass. **(d)** Short-axis T2-weighted image with fat suppression shows heterogeneous signal intensity of the mass. **(e)** Short-axis T2-weighted image with fat suppression shows heterogeneous signal intensity of the mass. **(f)** Short-axis contrast-enhanced fat-suppressed T1-weighted image shows heterogeneous enhancement of the mass.

Figure 3e. Congenital fibromatosis of the left foot in a 1-year-old girl. **(a)** Long-axis T1-weighted T2-weighted image shows a large soft tissue mass involving the medial aspect of the foot, with involvement of the adjacent bone. **(b)** Long-axis T1-weighted image after contrast enhancement shows heterogeneous enhancement of the mass. **(c)** Short-axis contrast-enhanced fat-suppressed T1-weighted image shows heterogeneous enhancement of the mass. **(d)** Short-axis T2-weighted image with fat suppression shows heterogeneous signal intensity of the mass. **(e)** Short-axis T2-weighted image with fat suppression shows heterogeneous signal intensity of the mass. **(f)** Short-axis contrast-enhanced fat-suppressed T1-weighted image shows heterogeneous enhancement of the mass.

Figure 3f. Congenital fibromatosis of the left foot in a 1-year-old girl. **(a)** Long-axis T1-weighted T2-weighted image shows a large soft tissue mass involving the medial aspect of the foot, with involvement of the adjacent bone. **(b)** Long-axis T1-weighted image after contrast enhancement shows heterogeneous enhancement of the mass. **(c)** Short-axis contrast-enhanced fat-suppressed T1-weighted image shows heterogeneous enhancement of the mass. **(d)** Short-axis T2-weighted image with fat suppression shows heterogeneous signal intensity of the mass. **(e)** Short-axis T2-weighted image with fat suppression shows heterogeneous signal intensity of the mass. **(f)** Short-axis contrast-enhanced fat-suppressed T1-weighted image shows heterogeneous enhancement of the mass.

Figure 3g. Congenital fibromatosis of the left foot in a 1-year-old girl. **(a)** Long-axis T1-weighted T2-weighted image shows a large soft tissue mass involving the medial aspect of the foot, with involvement of the adjacent bone. **(b)** Long-axis T1-weighted image after contrast enhancement shows heterogeneous enhancement of the mass. **(c)** Short-axis contrast-enhanced fat-suppressed T1-weighted image shows heterogeneous enhancement of the mass. **(d)** Short-axis T2-weighted image with fat suppression shows heterogeneous signal intensity of the mass. **(e)** Short-axis T2-weighted image with fat suppression shows heterogeneous signal intensity of the mass. **(f)** Short-axis contrast-enhanced fat-suppressed T1-weighted image shows heterogeneous enhancement of the mass.

Figure 3h. Congenital fibromatosis of the left foot in a 1-year-old girl. **(a)** Long-axis T1-weighted T2-weighted image shows a large soft tissue mass involving the medial aspect of the foot, with involvement of the adjacent bone. **(b)** Long-axis T1-weighted image after contrast enhancement shows heterogeneous enhancement of the mass. **(c)** Short-axis contrast-enhanced fat-suppressed T1-weighted image shows heterogeneous enhancement of the mass. **(d)** Short-axis T2-weighted image with fat suppression shows heterogeneous signal intensity of the mass.

Figure 12b. Congenital fibromatosis of the left foot in a 1-month-old boy. (**a**) Axial T1-weighted fast spin-echo image shows an irregular mass (*F*) with ill-defined margins involving the medial aspect of the foot, with invasion of the medial plantar fat (*P*) and the medial plantar neurovascular bundle (*arrowhead*). The fibrotic pattern and the presence of the medial plantar neurovascular bundle within the mass. (**b**) Short-axis contrast-enhanced fat-suppressed T1-weighted image shows enhancement of the mass (*F*). Image courtesy of Dr. Hon.

Download as PowerPoint | Open in Image Viewer

Multipotent MR Findings

Multipotent MR Findings.—At DWI, infantile fibromatosis usually shows diffusion restriction owing to its cellularity (Figure 12c). Tumor vascular supply is from areas where the tumor cannot be completely excised. DWI may be helpful in detecting tumor in proximity to surgical margins and residual disease.

Treatment.—If the tumor is confined to a specific region of the body, the mainstay therapy is surgical treatment with clear margins. However, when the neovascular bundle is involved, the tumor may be the entire extremity, amputation is indicated.

Compared with other soft-tissue sarcomas, infantile fibromatosis is more likely to recur after incomplete surgical resection (of 50% at 5 years [88,77]). Although local recurrence is relatively common, with a 50% rate in the first 2 years after resection, it is rarely fatal. Tumor recurrence is rare in the 5 years after resection and rates of disease at diagnosis are the most relevant prognostic factors.

Epithelioid Sarcoma

Epidemiologic Features.—Epithelioid sarcoma is a rare tumor that typically arises in the distal extremities of the upper limb and hand and in adolescents and young adults up to 35 years of age. Males are more frequently affected than females (2.5:1 ratio). Most tumors arise in the hand, fingers and hand but may also arise in other sites, including the musculature [75].

Although most epithelioid sarcoma manifests as a slow-growing painless mass, usually involving the fingers. When small, it may be mistaken for giant cell tumor of the tendon sheath or other benign lesions. Tumors may also frequently arising from the tendons and hand structures, may be misdiagnosed as synovial sarcoma or fibrosarcoma [78].

Histopathologic Findings.—There are two types of epithelioid sarcoma: the conventional or classic type, which is more common, and the proximal type, which typically affects slightly the deep tissue with tissue, more often in older people [75].

Tumor cells embrace immunoreactivity for epithelial markers, such as cytokeratin and EMA, and tumor cells show expression in characteristic [79]. Epithelioid sarcoma has a high rate of loss of INI1 (SMARCB1) gene, which is mostly expressed in the pathogenesis of most of these tumors.

Conventional MRI Findings.—Tumors are homogeneously isointense to muscle on T1-weighted images and homogeneously hyperintense to muscle on T2-weighted images with heterogeneous enhancement after administration of contrast material [75] (Fig. 13).

Figure 13a. Epithelioid sarcoma involving the subcutaneous soft tissues of the distal second right finger in a 15-year-old boy. (**a**) Sagittal fat-suppressed T2-weighted image shows a well-defined lobulated mass of homogeneous high signal intensity (*arrowheads*) with a central area of low signal intensity (*F*). There is absence of a cleavage plane between the flexor tendon (*arrow*) and the mass. (**b**) Axial contrast-enhanced fat-suppressed T1-weighted image shows diffuse intense enhancement of the mass (*F*), with small internal areas of hypointensity (*black arrowhead*) and a peripheral rim of enhancement (*white arrowheads*). Note the close relation of the mass to the flexor tendon (*white arrow*). (**c**) CT 3D image shows intense enhancement of the mass (*F*), with small internal areas of hypointensity (*black arrowhead*) suggestive of necrosis. Note the close relation of the mass to the flexor tendon (*white arrow*). (**d**) Photomicrograph of the surgical specimen shows a heterogeneous solid tumor (*F*) with areas of necrosis (*white arrow*) and hemorrhage (*black arrow*). (*F*=tendon).

Download as PowerPoint | Open in Image Viewer

Figure 13b. Epithelioid sarcoma involving the subcutaneous soft tissues of the distal second right finger in a 15-year-old boy. (**a**) Sagittal fat-suppressed T2-weighted image shows a well-defined lobulated mass of homogeneous high signal intensity (*arrowheads*) with a central area of low signal intensity (*F*). There is absence of a cleavage plane between the flexor tendon (*arrow*) and the mass. (**b**) Axial contrast-enhanced fat-suppressed T1-weighted image shows diffuse intense enhancement of the mass (*F*), with small internal areas of hypointensity (*black arrowhead*) and a peripheral rim of enhancement (*white arrowheads*). Note the close relation of the mass to the flexor tendon (*white arrow*). (**c**) CT 3D image shows intense enhancement of the mass (*F*), with small internal areas of hypointensity (*black arrowhead*) suggestive of necrosis. Note the close relation of the mass to the flexor tendon (*white arrow*). (**d**) Photomicrograph of the surgical specimen shows a heterogeneous solid tumor (*F*) with areas of necrosis (*white arrow*) and hemorrhage (*black arrow*). (*F*=tendon).

Download as PowerPoint | Open in Image Viewer

Figure 13c. Epithelioid sarcoma involving the subcutaneous soft tissues of the distal second right finger in a 15-year-old boy. (**a**) Sagittal fat-suppressed T2-weighted image shows a well-defined lobulated mass of homogeneous high signal intensity (*arrowheads*) with a central area of low signal intensity (*F*). There is absence of a cleavage plane between the flexor tendon (*arrow*) and the mass. (**b**) Axial contrast-enhanced fat-suppressed T1-weighted image shows diffuse intense enhancement of the mass (*F*), with small internal areas of hypointensity (*black arrowhead*) and a peripheral rim of enhancement (*white arrowheads*). Note the close relation of the mass to the flexor tendon (*white arrow*). (**c**) CT 3D image shows intense enhancement of the mass (*F*), with small internal areas of hypointensity (*black arrowhead*) suggestive of necrosis. Note the close relation of the mass to the flexor tendon (*white arrow*). (**d**) Photomicrograph of the surgical specimen shows a heterogeneous solid tumor (*F*) with areas of necrosis (*white arrow*) and hemorrhage (*black arrow*). (*F*=tendon).

Download as PowerPoint | Open in Image Viewer

Multipotent MR Findings.—Epithelioid sarcomas are highly cellular tumors and usually show restricted diffusion (Figure 13d). Tumor vascular supply is from areas where it cannot be completely excised. DWI may be helpful in detecting tumor in proximity to surgical margins and residual disease. Use of DWI and DCE MRI after tumor excision is mandatory to evaluate for recurrence.

Treatment.—Surgery is the mainstay of treatment, followed by adjuvant radiotherapy. Because of the frequent presence of both surgical margins, epithelioid sarcoma has a high rate of local recurrence with a tendency to metastasize to regional lymph nodes [80].

Extravasal Malignant Rhabdoid Tumor

Epidemiologic Features.—Malignant rhabdoid tumor is an aggressive pediatric sarcoma that was initially described in the kidneys by Beckwith and Palmer [75] in 1978 as an aggressive variant of Wilms tumor. Extravasal malignant rhabdoid tumor can be divided into two subtypes and subtypes differ according to its site of origin.

The extravasal malignant rhabdoid tumor is an exceedingly rare tumor that has been reported in adults at a prevalence of 11 months, but it may manifest in early infancy or late childhood [81]. It is a highly aggressive tumor with poor outcome, where it is also called atypical teratoid/rhabdoid tumor [78]. It can also occur in the soft tissues of the extremities and trunk [82].

Unlike soft-rhabdoid tumor involving the central nervous system, there is scarce literature on soft-tissue rhabdoid tumor, and most of the literature is based on case reports, mainly except for a series of nine well documented cases described by Garcia-Rigo et al [79].

Clinical Features.—As with other soft-tissue sarcomas, the clinical manifestation varies depending on the site of origin, but it typically presents as a painless mass with local compression of the surrounding structures [79].

Histopathologic Findings.—The most characteristic histopathologic features are rhabdoid cytomorphology, large vesicular nuclei, prominent nucleoli, and abundant cytoplasm [79]. Rhabdoid tumor commonly exhibits necrosis, hemorrhage, and calcification. Immunohistochemical expression is characteristically lost in extravasal rhabdoid tumor, as in the central nervous system tumor [79].

Conventional MRI Findings.—Extravasal malignant rhabdoid tumor often manifests as a large heterogeneous mass, hypo- to isointense to muscle on T1-weighted images and heterogeneously hyperintense to muscle on T2-weighted images. In some cases, it may have a cystic central component due to necrosis, reflecting its rapid growth (Fig 14a).

Figure 14a. Extravasal rhabdoid tumor in a newborn. (**a**) Sagittal T2-weighted image shows a large mass involving the subcutaneous fat at the posterior aspect of the neck. There is a peripheral inhomogeneous hypointense component (*arrows*) and an internal hyperintense area (*F*) that may reflect chronic hemorrhage. (**b**, **c**) Axial diffusion-weighted (**b**) and ADC (**c**) images show restricted diffusion in the peripheral and central components (*arrows*). (**d**, **e**) Axial contrast-enhanced fat-suppressed T1-weighted image shows intense peripheral enhancement from volumetric determination shows that the ADC of the mass (*arrows*) with no enhancement of the more central component (*F*), which owing to its low signal intensity on the T2-weighted image likely represents hemorrhage.

Download as PowerPoint | Open in Image Viewer

Figure 14b. Extravasal rhabdoid tumor in a newborn. (**a**) Sagittal T2-weighted image shows a large mass involving the subcutaneous fat at the posterior aspect of the neck. There is a peripheral inhomogeneous hypointense component (*arrows*) and an internal hyperintense area (*F*) that may reflect chronic hemorrhage. (**b**, **c**) Axial diffusion-weighted (**b**) and ADC (**c**) images show restricted diffusion in the peripheral and central components (*arrows*). (**d**, **e**) Axial contrast-enhanced fat-suppressed T1-weighted image shows intense peripheral enhancement from volumetric determination shows that the ADC of the mass (*arrows*) with no enhancement of the more central component (*F*), which owing to its low signal intensity on the T2-weighted image likely represents hemorrhage.

Download as PowerPoint | Open in Image Viewer

Figure 14c. Extravasal rhabdoid tumor in a newborn. (**a**) Sagittal T2-weighted image shows a large mass involving the subcutaneous fat at the posterior aspect of the neck. There is a peripheral inhomogeneous hypointense component (*arrows*) and an internal hyperintense area (*F*) that may reflect chronic hemorrhage. (**b**, **c**) Axial diffusion-weighted (**b**) and ADC (**c**) images show restricted diffusion in the peripheral and central components (*arrows*). (**d**, **e**) Axial contrast-enhanced fat-suppressed T1-weighted image shows intense peripheral enhancement from volumetric determination shows that the ADC of the mass (*arrows*) with no enhancement of the more central component (*F*), which owing to its low signal intensity on the T2-weighted image likely represents hemorrhage.

Download as PowerPoint | Open in Image Viewer

Figure 14d. Extravasal rhabdoid tumor in a newborn. (**a**) Sagittal T2-weighted image shows a large mass involving the subcutaneous fat at the posterior aspect of the neck. There is a peripheral inhomogeneous hypointense component (*arrows*) and an internal hyperintense area (*F*) that may reflect chronic hemorrhage. (**b**, **c**) Axial diffusion-weighted (**b**) and ADC (**c**) images show restricted diffusion in the peripheral and central components (*arrows*). (**d**, **e**) Axial contrast-enhanced fat-suppressed T1-weighted image shows intense peripheral enhancement from volumetric determination shows that the ADC of the mass (*arrows*) with no enhancement of the more central component (*F*), which owing to its low signal intensity on the T2-weighted image likely represents hemorrhage.

Download as PowerPoint | Open in Image Viewer

Figure 15a. Extravasal rhabdoid tumor in a newborn. (**a**) Sagittal T2-weighted image shows a large mass involving the subcutaneous fat at the posterior aspect of the neck. There is a peripheral inhomogeneous hypointense component (*arrows*) and an internal hyperintense area (*F*) that may reflect chronic hemorrhage. (**b**, **c**) Axial diffusion-weighted (**b**) and ADC (**c**) images show restricted diffusion in the peripheral and central components (*arrows*). (**d**, **e**) Axial contrast-enhanced fat-suppressed T1-weighted image shows intense peripheral enhancement from volumetric determination shows that the ADC of the mass (*arrows*) with no enhancement of the more central component (*F*), which owing to its low signal intensity on the T2-weighted image likely represents hemorrhage.

Download as PowerPoint | Open in Image Viewer

Figure 15b. Extravasal rhabdoid tumor in a newborn. (**a**) Sagittal T2-weighted image shows a large mass involving the subcutaneous fat at the posterior aspect of the neck. There is a peripheral inhomogeneous hypointense component (*arrows*) and an internal hyperintense area (*F*) that may reflect chronic hemorrhage. (**b**, **c**) Axial diffusion-weighted (**b**) and ADC (**c**) images show restricted diffusion in the peripheral and central components (*arrows*). (**d**, **e**) Axial contrast-enhanced fat-suppressed T1-weighted image shows intense peripheral enhancement from volumetric determination shows that the ADC of the mass (*arrows*) with no enhancement of the more central component (*F*), which owing to its low signal intensity on the T2-weighted image likely represents hemorrhage.

Download as PowerPoint | Open in Image Viewer

Figure 15c. Extravasal rhabdoid tumor in a newborn. (**a**) Sagittal T2-weighted image shows a large mass involving the subcutaneous fat at the posterior aspect of the neck. There is a peripheral inhomogeneous hypointense component (*arrows*) and an internal hyperintense area (*F*) that may reflect chronic hemorrhage. (**b**, **c**) Axial diffusion-weighted (**b**) and ADC (**c**) images show restricted diffusion in the peripheral and central components (*arrows*). (**d**, **e**) Axial contrast-enhanced fat-suppressed T1-weighted image shows intense peripheral enhancement from volumetric determination shows that the ADC of the mass (*arrows*) with no enhancement of the more central component (*F*), which owing to its low signal intensity on the T2-weighted image likely represents hemorrhage.

Download as PowerPoint | Open in Image Viewer

Multipotent MR Findings.—At DWI, solid areas show diffusion restriction. At DCE MRI, the tumor shows solid enhancement with internal areas of hypointensity consistent with a type III or IV tumor profile and areas of low signal intensity corresponding to necrosis, which correlates with a high ADC value. Tumor vascular supply is from areas leading surrounding structures [79].

Treatment.—Treatment includes radiation therapy to all tumor bed and surrounding lymphatic drainage, with surgery depending on the location of the tumor. However, the prognosis is poor, and the survival rate at 5 years is less than 10% regardless of the therapy used [79].

Conclusion

Use of unusualness MRI together with multiparametric MRI techniques provides additional data for detection, characterization, and staging of soft-tissue tumors and for follow-up during and after treatment. Advanced multiparametric MRI may have prognostic value in predicting tumor response to neoadjuvant treatment and recurrence and in evaluating residual disease after surgery.

Rhabdomyosarcoma is the most frequent soft-tissue sarcoma in children, and it is characterized by the most prominent and well-a better prognosis. MPMRI offer manifestos as peripheral leadoe enhancement and restricted diffusion. Most of the time, the differentiation between sarcoma is the second most common soft-tissue tumor in children and adolescents. Most of the time, it is a mixed-signal intensity sign on T2-weighted images, which is highly specific for malignancy. Most of the time, it is a mixed-signal intensity sign on T2-weighted images, which is highly specific for malignancy. Most of the time, it is a mixed-signal intensity sign on T2-weighted images, which is highly specific.

As a general rule, soft-tissue sarcomas usually manifest with restricted diffusion and a type III or IV tumor profile. In the setting of a known malignancy, the presence of an associated cystic profile is type I fibrosis and granulation tissue, which is a benign tumor profile.

Disclosures of Conflicts of Interest.—**J.W.C.** Activities related to the present article: disclosed no relevant relationships. Activities not related to the present article: disclosed no other relationships. Other activities: disclosed no relevant relationships.

Presented as an educational exhibit at the 2019 RSNA Annual Meeting.

For this journal-based SA CME activity, the author (M.A.C.) and the editor (Richard Gunderman) have no relevant to the reviewers have disclosed no relevant relationships.

Article History

Received: Sep 17 2019
Revision requested: Jul 24 2019
Revision received: Nov 6 2019
Accepted: Sept 11 2019
Published online: Apr 20 2020
Updated online: Sept 2020

Recommended

Multiparametric Assessment of Treatment Response in High-Grade Soft Tissue Sarcoma: Preliminary Experience with Imaging Sequelae
Radiology: Volume 2 | Jul 2020

Musculoskeletal Tumors: Tips and Tricks in Imaging Diagnosis and Metastatic Bone Disease
Radiology: Volume 292 | Sep 2019

CT and MRI Imaging of Primary Cardiac Malignancies
Radiographics | Nov 2020

Tumor vascular, location should guide MRI surveillance after soft tissue sarcoma resection?
Radiology: Volume 292 | Sep 2019

Deformation-Based Morphometry Reveals Sarcomas
Radiology: Volume 292 | Sep 2019

Glycogen synthase kinase 3 beta inhibitor tideglusib suppresses fibrosis in Duchenne muscular dystrophy
Ann Rheum Dis | Jul 2020

Comment by Dr. Gunderman on Tideglusib and Duchenne Muscular Dystrophy
JCR